Available online at www.sciencedirect.com
SCIENCE DIRECT®
International Journal of Thermal Sciences 43 (2004) 623–630
International Journal of Thermal Sciences
www.elsevier.com/locate/ijts

Trans-critical R744 and two-phase flow through short tube orifices ☆

J.P. Chen *, J.P. Liu, Z.J. Chen, Y.M. Niu

Institute of Refrigeration and Cryogenics, Shanghai Jiaotong University, Huashan Road 1954, Shanghai 200030, People's Republic of China

Received 17 June 2003; accepted 28 October 2003

Available online 10 January 2004

Abstract

In trans-critical R744 refrigeration system, the flow of refrigerant through a short tube orifice is greatly different from that of a conventional refrigerant such as R134a. A specially designed short tube orifice was used to investigate the two-phase flow inside tube. Experimental results indicated that choked flow existed in all cases. The location of flashing inception within the tube would move to the exit as the upstream pressure increased.

The relationships between the mass flow rate and the independent variables such as upstream pressure, upstream temperature, short-tube diameter and length were also examined. The R744 mass flow rate was strongly dependent on the diameter, and was proportional to the upstream pressure. A correlation that could be used to predict the mass flow rate was developed based on a large of experimental data. Approximately 95% of the measured data were within ±6% of the prediction. The maximum error between the measured data and the calculated results was within 16%.

Keywords: Short tube orifice; Two-phase flow; R744; Refrigeration; Trans-critical cycle; Critical flow

1. Introduction

The two-phase flow through a short tube orifice is rather complicated although its geometries are simple. A choking phenomenon was observed for refrigerants flowing through short tube orifices by several previous researchers [1–12]. When this happened, the mass flow rate was almost independent of the downstream pressure. This indicated that the flow through a short tube orifice under choked flow conditions generally corresponded to the critical flow. There are many uncertainties about the physics in two-phase critical flow, and it is difficult to find a general theoretical model to predict the mass flow rate accurately.

Previous work mainly focused on initially subcooled, two-phase or saturated fluids at the entrance. Baily [1] investigated the flow of saturated and nearly saturated water flowing through short tube orifices. From his experimental results, the flow region could be divided into three distinct regimes. When the downstream pressure was considerably less than P_{sat}, the choking flow occurred. Zaloudek [2] found the same flow curves when he studied water flowing through short tube orifices. However, Zaloudek [2] observed no difference in the mass flow rate from the transition between the first and second regime, and hence termed the phenomenon as the first-stage choking. The choking regime in Baily's study was termed as the second-stage choking. Pasqua [4] studied the flow of subcooled and saturated liquid R12 flowing through short tube orifices. He concluded that a metastable liquid core increased the flow rate compared to when the flow flashed inside the tube. For R22, Mei [5] observed first-stage choking at the liquid subcooling temperature of 22.2 °C but no indication of second-stage choking. Krakow and Lin [6] also observed that the flow of R12 through short tube orifices was choked. Simões-Moreira and Bullard [12] examined a novel pressure drop mechanism in refrigerant expansion devices, and suggested that the evaporation wave may be the flow controlling mechanism in these devices.

The pressure profiles of refrigerants inside a short tube orifice were similar to the capillary tube flow. There existed a large pressure drop at the entrance and outlet of tube, respectively. For initially subcooled refrigerants, the pressure at the first tap (entrance of the tube) was already lower than

☆ This study was supported by Nature Science Fund Committee of China and Shanghai Automotive Industry Group.

* Corresponding author.
E-mail address: jeepliu@sjtu.edu.cn (J.P. Liu).

1290-0729/$ – see front matter
doi:10.1016/j.ijthermalsci.2003.10.011

Nomenclature

A_s	short tube cross-sectional area	m^2	
D	short tube diameter	mm	
D_{ref}	reference short-tube diameter	(1.35)	mm
D_R	normalized diameter, $= D/D_{ref}$		
L	short tube length	mm	
L/D	ratio between short-tube length and diameter		
$\dot{m}$	mass flow rate	$kg \cdot h^{-1}$	
$\dot{m}_{averg}$	average value of all the mass flow rates at different downstream pressure with the same upstream conditions	$kg \cdot h^{-1}$	
P_c	critical pressure	(7.38)	MPa
P_{down}	downstream pressure		MPa
P_f	adjusted downstream pressure		MPa
$P_{l,averg}$	average pressure through the entire short tube orifice		
P_R	normalized upstream pressure, $= P_{up}/P_c$		
P_{sat}	saturation pressure corresponding to upstream temperature		MPa
$P_{sat,i}$	saturation pressure corresponding to the local temperature at the ith point		
P_{up}	upstream pressure		MPa
t_c	critical temperature	(31.03)	°C
t_R	normalized upstream temperature, $= (t_{up} - t_c)/t_c$		°C
t_{up}	upstream temperature		°C

Greek symbol

ρ	density	$kg \cdot m^{-3}$

Subscripts

averg	average
c	critical point
down	downstream of short tube
f	adjust parameter
R	normalized parameters
ref	reference
s	short tube orifice
sat	saturation condition
up	upstream of a short tube orifice

the saturated pressure corresponding to the upstream temperature. The pressure recovered at the second or third tap as the refrigerant flowed, and then approached to the saturation pressure corresponding to the upstream temperature [7–11].

Most of the short-tube flow models have been developed by empirically correcting the orifice constant, C and downstream pressure, P_{down}, in the general orifice equation [7–11]. The experimental performance of short tubes has been well characterized for R12 and for R22. Kim and O'Neal [10] studied the flow of R134a through short tube orifices under a wide range of operating conditions and geometric configurations. A semi-empirical model was developed to predict the mass flow rate. Payne and O'Neal [9] undertook another relevant work, studying the flow characteristics of R407C experimentally through the sharp-edged tubes. Singh [11] developed a semi-empirical model based on an extensive set of measurements of mass flow rate of R-134a through orifice tubes in his study also.

There has been limited research addressing trans-critical or superheated fluid flowing through short tube orifices. In trans-critical R744 cycle proposed by Lorentzen [13], the upstream pressure and temperature were above its critical point (31 °C, 73.8 bar). The models or empirical charts available concerning refrigerants flowing through short tube orifices could not be used to predict the mass flow rate of R744 directly. Further, it is still unclear whether or not the R744 is choked within the normal operating conditions of a trans-critical cycle.

Several studies focused on components such as compressors [14], heat exchangers [15] and analyzed the performance of the trans-critical cycle. About the throttling devices, no literature could be found which studied the flow characteristics and the flashing mechanism of R744 flowing through the throttling devices.

In this paper, a short tube orifice was selected as the expansion and flow-rate-controlling device, and the R744 flowing through it was studied experimentally. The flow inside short tube was investigated through pressure profile observation tests. A semi-empirical correlation was obtained to predict the R744 mass flow rate through short tube orifices.

2. The different flow conditions

2.1. Experimental setup

All the tests were performed on a reformed CO_2 automobile air conditioning calorimeter. A schematic of the experimental loop is shown in Fig. 1. The setup used in this study consisted of three loops: a refrigeration loop including a detachable test section, a hot air flow loop used for the evaporation heat exchanger (evaporator room), and a air flow loop used for taking heat rejected from gas cooler (gas cooler room). The temperatures of the circulated air in both evaporator room and gas cooler room could be easily controlled using two room air conditioners and two electric heaters. Two induced fan frequency-converters were selected to adjust the volume of air flowing through the evaporator and gas cooler, and so the evaporating pressure and the temperature of R744 entering short tubes could be easily controlled. The flow rates can be measured by two nozzle systems.

The compressor was developed by a professional compressor company which cooperated with us. It can provide a

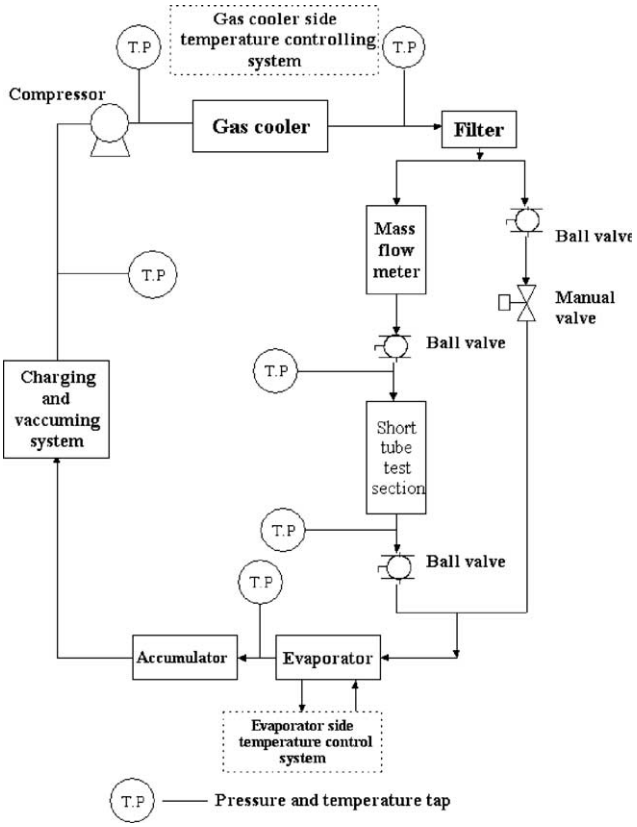

Fig. 1. Schematic diagram of the experimental setup for short tube tests.

wide range of refrigerant mass flow rates by a variable speed motor. Synthetic refrigerator oil RENISO 130E was used to lubricate the compressor. Because it was difficult to completely separate the oil from the refrigerant, oil separator was not installed in the system. So actually, R744-oil mixture flowing through the short tube orifice was investigated in this paper. The oil concentration was determined by sampling before beginning the flowing tests. At the normal operating conditions, the oil concentration ranged from 2.9 to 3.4%. Under the working conditions in our tests, the dynamic viscosity of the synthetic oil ranged from 50 to 85×10^{-6} Pa·s. A filter was installed before entering the short tube orifice to filter particles. The upstream pressure could be controlled by adjusting the speed of the compressor. A manual expansion valve was used to permit precise control of upstream pressure by bypassing part of high pressure fluid directly to the evaporator inlet. The downstream pressure could be controlled by adjusting the temperature and the volume of air flowing through the evaporator. The test section was designed to allow easy installation and removal of the different short tube orifices.

Pressure transducers were calibrated to an estimated accuracy of ±0.1% full-scale range (16 MPa). Experimental uncertainty of the temperature measurement was estimated at ±0.2 K. A coriolis mass flow meter was calibrated to an estimated accuracy of ±0.2% full-scale range (360 kg·h^{-1}) to measure the mass flow rate through short tube orifices.

Table 1
Dimensions of the short tubes tested in the present study

Short tube	Diameter		Length		Chamfer depth	Remarks
	[mm]	[In.]	[mm]	[In.]	[mm]	
1	1.34	0.0528	9.54	0.3756	Sharp-edged	
2	1.34	0.0528	12.70	0.5000	Sharp-edged	
3	1.13	0.0445	12.70	0.5000	Sharp-edged	
4	0.83	0.0327	12.76	0.5024	Sharp-edged	
5	1.53	0.0602	12.76	0.5024	Sharp-edged	
6	1.35	0.0532	25.42	1.0008	Sharp-edged	
7	1.35	0.0532	8.02	0.3157	Sharp-edged	
8	1.35	0.0532	11.20	0.4409	Sharp-edged	
9	1.35	0.0532	16.28	0.6409	Sharp-edged	
10	1.36	0.0535	20.44	0.8047	Sharp-edged	
11	1.35	0.0532	12.92	0.5087	Sharp-edged	Pressure profiles test

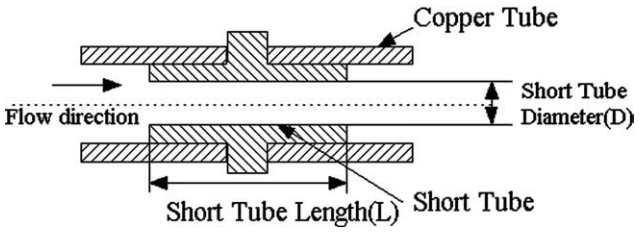

Fig. 2. Schematic diagram of the short tube tested.

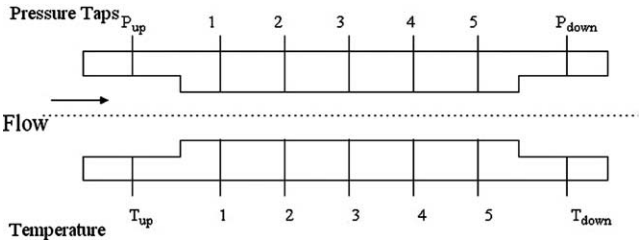

Fig. 3. Positions of pressure and temperature taps along the short tube.

Table 1 lists the short tube orifices used in this study. Those short tubes were manufactured from brass rods, and then fixed between two 7.03 mm diameter copper pipes using silver solder (shown in Fig. 2). Diameters were measured with a precise plug gauge set with 0.015 mm increment of diameter. Short tube lengths were measured with a dial caliper. The estimated accuracy of both diameter and length measurements were ±0.015 mm.

The pressure inside the short tube orifice was measured through a specially designed tube (Fig. 3). Along the short tube orifice, five pressure taps were bored to 0.10 ± 0.05 mm diameters using laser equipment to reduce their effects on mass flow rate. Mass flow rates at various upstream and downstream conditions were measured both before and after the pressure taps were bored. The differences were found to be within 1.5%, thus the pressure taps were assumed to have no appreciable effects on the flow rate. Two taps were bored to 0.50 ± 0.1 mm diameters immediately before and after the short tube to measure the upstream and downstream pressure. Corresponding to each

pressure measurement along the tube, five holes (2.0 mm diameter) were bored to install thermocouples to measure the local temperature. In order to avoid destroying the flow inside tube, all the thermocouples were not inserted into the tube. The test section was insulated from the surrounding environment using thermal insulating materials.

2.2. Testing conditions and procedure

The operating conditions were selected to cover the normal working conditions for automobile air conditioner. A series of tests were completed to study the effects of the operating parameters on mass flow rates through short tube orifices. The basic variables controlled were:

(1) upstream temperature,
(2) upstream pressure, and
(3) downstream pressure.

Each variable could be individually controlled while keeping the others constant. Upstream temperature was set at 35, 40 and 45 °C. Upstream pressure was set at 7.55, 8.55, 9.05, and 9.57 MPa, while downstream pressure was maintained constant at 3.52, 4.01, and 4.53 MPa. So totally 36 tests were performed on each short tube. The repeatability was checked by repeating the test with the same conditions as the first test. Thermodynamic properties of R744 were calculated through RefProp version 6.01.

3. Experimental results and discussions

3.1. Flow analysis inside the short tube orifice

An average pressure level index was define as:

$$P_{l,\text{averg}} = \frac{1}{5}\sum_{i=1}^{5} P_i \tag{3.1}$$

where $P_{l,\text{averg}}$ is the average pressure inside the tube and P_i is local pressure at each pressure measurement tap.

Pressure profiles are shown in Fig. 4 for the same inlet state at three different downstream pressures. Large pressure drops at the entrance of tube resulted from rapid fluid acceleration and abrupt contraction at the inlet. The pressure decreased gradually as flowing through the short tube, and did not tend to recover at each pressure tap. This was different from R134a flow, which the pressure inside the tube tended to recover at the second pressure tap. The large pressure drop at the exit plane indicated that the flow was fully expanded inside the tube. For single-phase fluids, a large pressure drop at the exit plane would indicate choking has occurred. For two-phase flow, one may conclude that the flow is approximately choked.

Another significant phenomenon found from Fig. 4 was that the reduction of downstream pressure nearly did not cause a drop in the pressure throughout the entire short tube orifice. This means that the downstream pressure wave is less than or at least equal the refrigerant velocity, and accordingly cannot communicate downstream information upstream. The R744 flowing through a short tube is more like a single-phase critical flow.

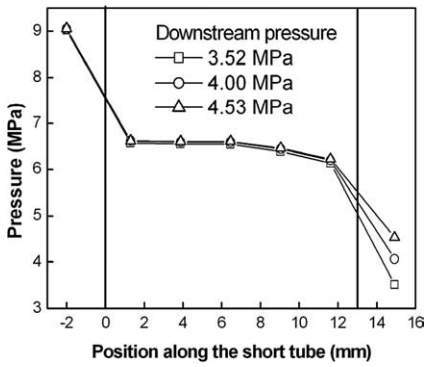

Fig. 4. Pressure profile along the short tube at various downstream pressures ($P_{\text{up}} = 9.05$ MPa, $t_{\text{up}} = 40.0$ °C).

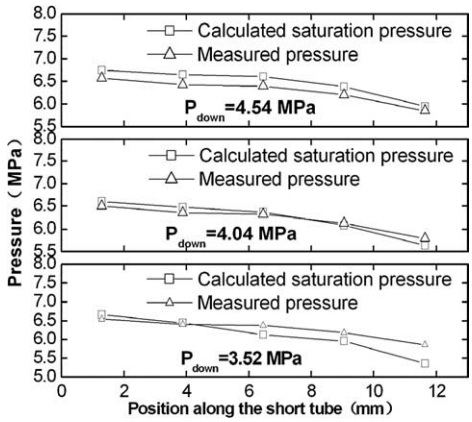

Fig. 5. Measured and saturated pressure profile along the short tube ($P_{\text{up}} = 9.05$ MPa, $T_{\text{up}} = 40$ °C).

The reduction of downstream pressure caused a slight drop in temperature profile, although it did not cause a pressure drop inside the tube (Fig. 5). Nearly all the saturation pressures $P_{\text{sat},i}$ corresponding to the temperature at each point were higher than the local measured pressures when the downstream pressure was 3.52 MPa. As the downstream pressure increased to 4.53 MPa, all measured pressures were lower than the local $P_{\text{sat},i}$.

Fig. 6 shows the pressure profile of the short tube orifice with upstream temperature and downstream pressure constant while the upstream pressure was varied. Clearly, the average pressure level $P_{l,\text{averg}}$ inside the tube increased as the upstream pressure increased. Combining the relationship between the mass flow rate and upstream pressure shown in Fig. 12, one may conclude that the value of $P_{l,\text{averg}}$ defines the mass flow rates through short tube orifice.

As the upstream pressure was low (e.g., 7.55 or 8.55 MPa), the refrigerant began to flash at the third or forth point

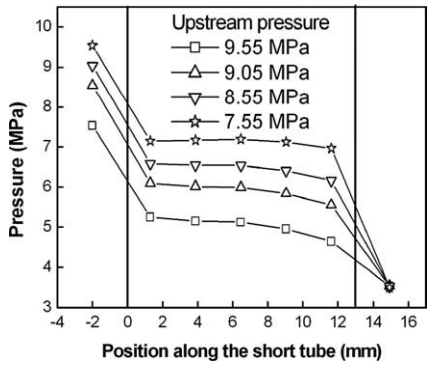

Fig. 6. Pressure profile along the short tube at various upstream temperatures ($t_{up} = 35.3\,^{\circ}C$, $P_{down} = 3.52$ MPa).

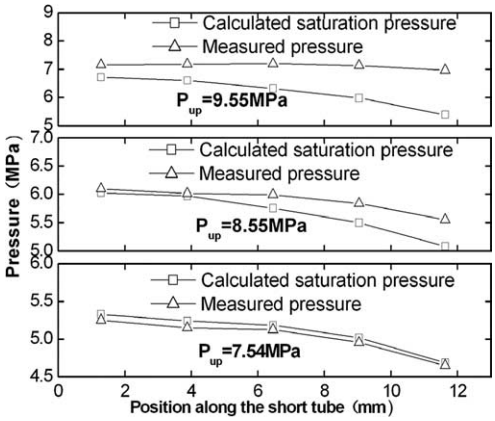

Fig. 7. Measured and saturated pressure profile along the short tube ($t_{up} = 35.3\,^{\circ}C$, $P_{down} = 3.5$ MPa °C).

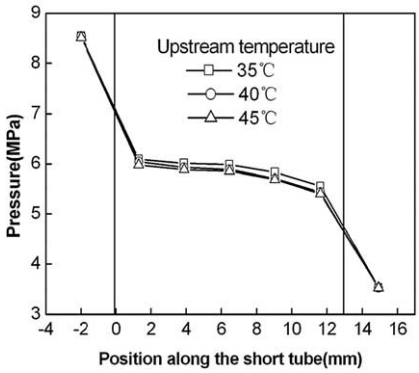

Fig. 8. Pressure profile along the short tube at various upstream temperatures ($P_{up} = 8.55$ MPa, $P_{down} = 3.52$ MPa).

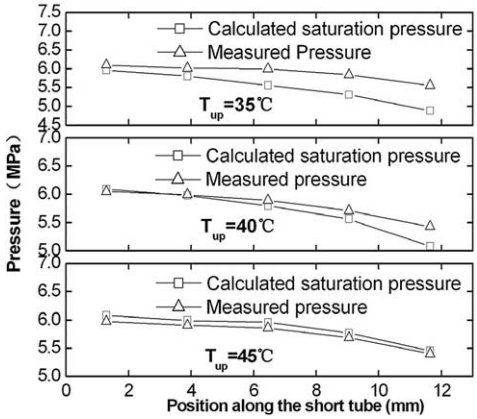

Fig. 9. Measured and saturated pressure profile along the short tube ($P_{up} = 8.55$ MPa, $P_{down} = 3.52$ MPa).

when it flowed through entire tube. This could be identified from the abruptly larger pressure drop than before. When this happened, the pressure drop was the sum of the friction and flashing acceleration pressure drop. Flashing only began to occur near the exit plane of the short tube orifice when the upstream pressure was increased to 9.05 MPa. As the upstream pressure was increased to 9.5 MPa, the pressure drop along the short tube was only 0.183 MPa. All measured pressures at each point were higher than the saturation pressures $P_{sat,i}$ corresponding to the temperature (Fig. 7). This indicates that flashing does not occur inside the tube, and single-phase liquid flows through the entire short tube.

The pressure drop decreased from 0.602 to 0.423 MPa when the upstream pressure was increased from 7.55 to 9.05 MPa. This indicates that the location of flashing inception within the tube moves to the exit plane. The location of flashing inception within the tube constitutes the origin of the time scale for bubble growth, thereby serving as the initial condition for the calculation of the vapor generation rate. Thus, flashing inception occurring upstream of the exit (critical plane) tends to increase the void fraction at the exit and hence, the compressibility of the flow. This will result in a lower critical mass flux exiting the tube.

Fig. 8 shows the pressure profile with upstream and downstream pressures constant while the upstream temperature was varied. The average pressure level $P_{l,averg}$ decreased as the upstream temperature was increased. As the upstream temperature increased from 35 to 40 °C, the variation of the average pressure level was greatly higher than the variation while the upstream temperature increasing from 40 to 45 °C. The trend consisted with the relationships between the mass flow rate and the upstream temperature found in Fig. 11. The location of flashing inception moved to the upstream when the upstream temperature increased from 35 to 45 °C (seen from Fig. 9). The effect of increasing upstream temperature on mass flow rate is similar to decreasing inlet subcooling of R134a flowing through short tube orifices.

3.2. Flow characteristics through short tube orifices

Effects of downstream pressure

Fig. 10 shows the variation of mass flow rates with downstream pressure at different upstream pressures. The upstream temperature was maintained constant at 35.2 °C. As the downstream increased from 3.55 to 4.53 MPa, the mass flow rate remained nearly constant. The amplitudes of variation were less than ±2% compared to the average mass flow rate $\dot{m}_{averg}$ which was defined as the average value of mass flow rates at different downstream pressure with the

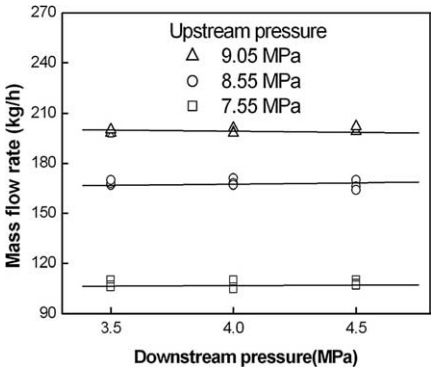

Fig. 10. Experimental mass flow rate vs. downstream pressure for short tube tested ($L = 12.92$ mm, $D = 1.35$ mm, $t_{up} = 35.2\,^{\circ}$C).

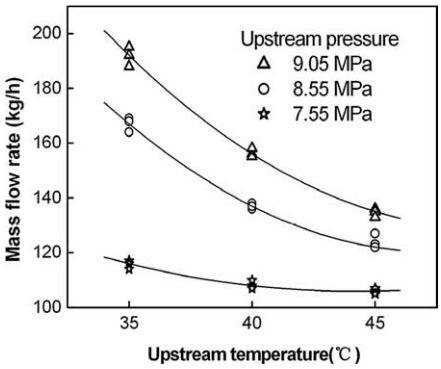

Fig. 11. Experimental mass flow rate vs. upstream temperature for short tube tested ($L = 25.42$ mm, $D = 1.35$ mm, $P_{down} = 3.52$ MPa).

Table 2
Values of exponent C_1, C_2 and the variations of mass flow rate

Upstream pressure P_{up} [MPa]	Coefficient C_1	Exponent C_2	Variations of mass flow rate [%]	
			35–40 °C	40–45 °C
7.55	99.23	−0.0744	−6.3	−2.2
8.55	99.23	−0.2601	−18.0	−7.5
9.05	99.23	−0.3374	−18.6	−13.7

same upstream conditions. Those indicated that the mass flow rate was insensitive to the downstream pressure, and that choking flow conditions were established as refrigerant CO_2 flowed through short tube orifices.

Effects of upstream temperature

Fig. 11 shows the results of mass flow rate as a function of upstream temperature at different upstream pressures. The downstream pressure was maintained constant. The negative exponential relationship between the mass flow rate and the upstream temperature was observed from those experimental results. The experimental data were correlated to Eq. (3.1). Coefficient C_1 was maintained constant. Exponent C_2 strongly depended upon the upstream pressure. The values of C_1 and C_2 were listed in Table 2. As the temperature was increased from 40 to 45 °C, the variation in mass flow rate was small compared to when it was increased from 35 to 40 °C (seen from Table 2).

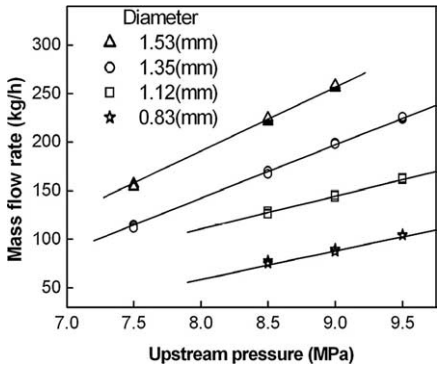

Fig. 12. Mass flow rate vs. upstream pressure ($t_{up} = 35.3\,^{\circ}$C, $P_{down} = 3.52$ MPa).

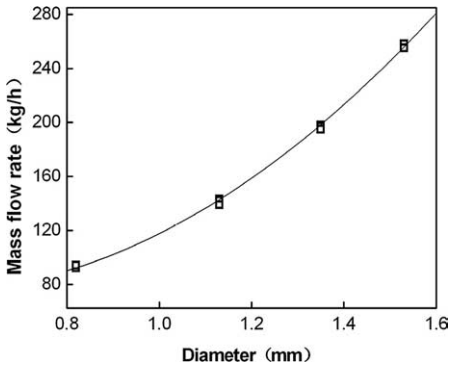

Fig. 13. Mass flow rate vs. short-tube diameter ($L = 12.74$ mm, $P_{up} = 9.05$ MPa, $P_{down} = 3.52$ MPa, $t_{up} = 35.2\,^{\circ}$C).

$$\dot{m} = C_1 \times (t_R)^{C_2} \tag{3.2}$$

where C_1 was a coefficient, C_2 was an exponent, $t_R = (t_{up-t_c})/t_c$ (P_c, t_c are the critical pressure and temperature of R744, respectively) and $\dot{m}$ is the mass flow rate of R744.

Effects of upstream pressure

Fig. 12 shows the variation of CO_2 mass flow rate with upstream pressure for different short-tube diameters. For each short tube orifice, the mass flow rate was directly proportional to the upstream pressure. The slope of each nearly linear line was slightly dependent on the short tube diameter. As the diameter increased, the lines tended to diverge from one another.

Effects of short-tube diameter

Fig. 13 shows the experimental mass flow rate as a function of short tube diameter. The upstream and downstream pressure was 9.05 and 3.52 MPa, respectively. The experimental data were correlated to Eq. (3.2). The exponent c was found to be 2.73 for sharp-edged short tube orifices, and was greater than R22 (2.11) [7] and, R134a (1.9)–(2.4) [10].

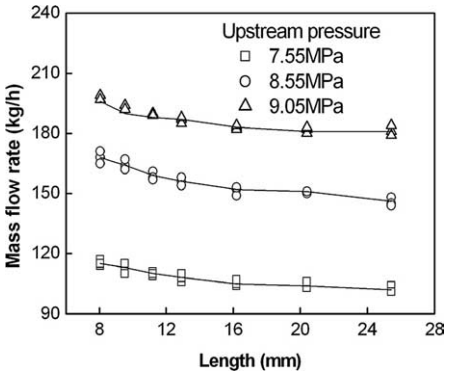

Fig. 14. Mass flow rate vs. short-tube length ($D = 1.35$ mm, $t_{up} = 35.2\,^{\circ}$C, $P_{down} = 3.52$ MPa).

This indicates that the diameter strongly influences the mass flow rate of R744 flowing through a short tube.

$$\dot{m} = a + b \times (D)^C \tag{3.3}$$

where coefficients $a = 55.43$ and $b = 66.72$, c was an exponent and D was the diameter of short tube orifices. The units of D and $\dot{m}$ were mm and kg·h^{-1}, respectively.

Effects of short-tube length

Fig. 14 shows the dependency upon short-tube length at different upstream pressure. The relationship between mass flow rate and short-tube length was similar to R22 flow. As the tube length was increased from 12.74 to 25.44 mm, the mass flow variation was small compared to when it was decreased from 12.74 to 8.05 mm. The maximum mass flow rate variation was within 10% as the short-tube length was increased.

4. Short-tube mass flow model

Based on the relationship between mass flow rate and downstream pressure observed in our tests, the two-phase R744 flow through a short tube orifice was critical flow. A critical model based on sonic velocity would be appropriate to describe the flow. But the fluid quality, temperature and sonic velocity inside short tubes could not be successfully predicted. Thus, it was difficult to derive a critical flow model for R744 flowing through a short tube.

The single-phase orifice equation (Eq. (4.1)) was usually corrected to predict the two-phase flow through a short tube [7–10].

$$\dot{m} = A_s \cdot \sqrt{2 \cdot \rho \cdot (P_{up} - P_f)} \tag{4.1}$$

where P_f is adjusted downstream pressure, ρ is density of upstream fluid entering short tube and A_s is cross-sectional area of the short tube.

The variable P_f was correlated with upstream temperature, upstream pressure, D and L/D. The P_c was used as a reference value for P_f. All the corrections to P_f were nondimensional. The nondimensional parameter $(t_{up} - t_c)/t_c$ was used to evaluate the effect of upstream temperature, and the dependency on upstream pressure was correlated with the normalized upstream pressure, P_{up}/P_c. The relationships with geometric parameters were correlated with the ratio L/D and D/D_{ref}. Short tube orifice with diameter 1.35 mm was selected as the reference tube diameter D_{ref}.

Using a nonlinear curve-fitting method, the following expression for the adjusted downstream pressure for sharp-edged entrance short tubes was obtained as:

$$\begin{aligned} P_f = P_c | & 1.17344 + 0.0306 D_R^{3.70318} \\ & - 0.37139 P_R^{-4.29588} t_R^{0.03813} \\ & + 0.00002 (L/D)^{2.13404} \end{aligned} \tag{4.2}$$

where $D_R = D/D_{ref}$ ($D_{ref} = 1.35$ mm), $P_R = P_{up}/P_c$ and $t_R = (t_{up} - t_c)/t_c$ (P_c, t_c are the critical pressure and temperature of R744, respectively).

Using Eqs. (4.1) and (4.2), the mass flow rate of R744 through short tube orifices could be predicted under the given operating conditions and short-tube geometries. Approximately 95% of the measured data were within ±6% of the prediction. The maximum error between the measured data and the calculated results were within 16%. The model should be used with cautions for conditions outside the range of variables used in developing the model. For refrigerant CO_2, two-phase or liquid refrigerant entering the short tube were not considered in this study. The range of diameters and lengths can be referred from the list of short tubes in Table 1. Table 2 listed the ranges of upstream pressure, downstream pressure and upstream temperature. The effects of oil contamination should be investigated in detail later. Some variables such as downstream pressure, inlet and outlet chamfer were not included in this model because of their weak effects on mass flow rate observed from experimental results.

5. Conclusions

Trans-critical R744 flow through short tube orifice was greatly different from R22 flow. Choking flow happened within a wide range of working conditions of trans-critical R744 automobile air conditioning system. The reduction of downstream pressure did not cause a drop in pressure throughout the entire short tube, which meant critical two-phase flow occurring.

The trans-critical fluid was not always directly throttled into two-phase region. The pressure drop inside the short tube orifice decreased when the upstream pressure increased, which indicated that the location of flashing inception moved to the exit plane of tube. As the upstream pressure increased to 9.55 MPa, no vaporization happened inside the short tube orifice. The flow inside the tube maintained single-phase liquid flow.

The average pressure level increased when the upstream pressure increased. This will resulted in a higher critical mass flow rate exiting the tube. The mass flow rate was directly proportional to the upstream pressure. The pressure $P_{l,averg}$ decreased when the upstream temperature increased.

The mass flow rate decayed with a negative exponent when the upstream temperature increased.

The mass flow rate was proportional to the cross-sectional area of short tube, and the exponent (2.73) was greater than R22 (2.11) [7] and, R134a (1.9)–(2.4) [10]. The relationship between the mass flow rate and the length was similar to which of R22.

Using the model developed in this paper, the predictions of mass flow rate fit the experimental data well for a wide automobile air conditioning operating conditions and a number of short-tube geometries.

Appendix A

Table A.1
Pressure distribution along the short tube orifice

No.	T_{up} [K]	P_{up} [MPa]	P_1 [MPa]	P_2 [MPa]	P_3 [MPa]	P_4 [MPa]	P_5 [MPa]	P_{down} [MPa]
1	313.1	9.06	6.55	6.40	6.37	6.18	5.86	3.53
2	313.1	9.01	6.50	6.35	6.32	6.13	5.79	3.99
3	313.1	9.06	6.57	6.42	6.39	6.20	5.86	4.51
4	308.4	7.54	5.25	5.15	5.12	4.95	4.65	3.53
5	308.4	8.54	6.09	6.01	5.99	5.84	5.55	3.54
6	308.4	9.04	6.58	6.54	6.54	6.40	6.16	3.53
7	308.4	9.53	7.15	7.17	7.19	7.12	6.96	3.50
8	308.3	8.54	6.09	6.01	5.99	5.84	5.55	3.54
9	313.2	8.54	6.04	5.93	5.89	5.70	5.43	3.53
10	318.4	8.51	5.98	5.88	5.85	5.69	5.40	3.53

Table A.2
Saturated pressure (temperature) distribution along short tube orifice

No.	T_{up} [K]	P_{up} [MPa]	P_1 [MPa]	P_2 [MPa]	P_3 [MPa]	P_4 [MPa]	P_5 [MPa]	P_{down} [MPa]
1	313.1	9.06	6.65	6.44	6.12	5.96	5.36	3.53
2	313.1	9.01	6.61	6.47	6.37	6.08	5.63	3.99
3	313.1	9.06	6.74	6.65	6.61	6.38	5.94	4.51
4	308.4	7.54	5.33	5.24	5.18	5.02	4.68	3.53
5	308.4	8.54	5.83	5.73	5.70	5.52	5.20	3.54
6	308.4	9.53	6.71	6.59	6.31	5.97	5.40	3.50
7	308.3	8.54	5.95	5.80	5.55	5.30	4.88	3.54
8	313.2	8.54	6.08	5.98	5.79	5.56	5.08	3.53
9	318.4	8.51	6.08	5.99	5.96	5.77	5.45	3.53

Table A.3
Mass flow rate at different flowing conditions

No.	L [mm]	D [mm]	T_{up} [K]	P_{up} [MPa]	P_{down} [MPa]	Average mass flow rate [kg·h^{-1}]
1	12.92	1.35	308.3	7.55	3.52	107.7
2	12.92	1.35	308.3	7.55	4.05	107.0
3	12.92	1.35	308.3	7.55	4.53	108.3
4	12.92	1.35	308.3	8.55	3.52	168.3
5	12.92	1.35	308.3	8.55	4.05	168.6
6	12.92	1.35	308.3	8.55	4.53	166.7
7	12.92	1.35	308.3	9.05	3.52	198.3
8	12.92	1.35	308.3	9.05	4.05	199.7
9	12.92	1.35	308.3	9.05	4.53	200.3
10	25.42	1.35	308.3	7.55	3.52	115.7
11	25.42	1.35	313.4	7.55	3.52	108.3
12	25.42	1.35	318.3	7.55	3.52	106.0
13	25.42	1.35	308.3	8.55	3.52	167.0
14	25.42	1.35	313.4	8.55	3.52	137.3
15	25.42	1.35	318.3	8.55	3.52	124.0
16	25.42	1.35	308.3	9.05	3.52	192.0
17	25.42	1.35	313.4	9.05	3.52	156.0
18	25.42	1.35	318.3	9.05	3.52	134.7
19	12.74	0.82	308.3	9.05	3.52	93.7
20	12.74	1.13	308.3	9.05	3.52	141.3
21	12.74	1.35	308.3	9.05	3.52	196.7
22	12.74	1.53	308.3	9.05	3.52	256.3
23	8.05	1.35	308.3	7.55	3.52	115.2
24	9.54	1.35	308.3	7.55	3.52	113.0
25	11.2	1.35	308.3	7.55	3.52	110.0
26	16.2	1.35	308.3	7.55	3.52	105.1
27	20.4	1.35	308.3	7.55	3.52	104.3

References

[1] J.F. Baily, Metastable flow of saturated water, Trans. ASME 73 (1951) 1109–1116.

[2] F.R. Zaloudek, The critical flow of hot water through short tubes, HW-77594, Hanford Works, 1963.

[3] R.L. Collins, Choked expansion of subcooled water and the I.H.E. flow model, J. Heat Transfer 100 (5) (1978) 275–279.

[4] P.F. Pasqua, Metastable flow of freon-12, Refrig. Engrg. 61 (1953) 1084–1088.

[5] V.C. Mei, Short tube refrigerant flow restrictors, ASHRAE Trans. 88 (2) (1982) 157–169.

[6] K.I. Krakow, S. Lin, Refrigerant flow through orifices, ASHRAE Trans. 94 (1) (1988) 484–506.

[7] A.A. Aaron, P.A. Domanski, Experimentation, analysis, and correlation of Refrigerant-22 flow through short tube restrictors, ASHRAE Trans. 96 (1) (1990) 729–742.

[8] Y. Kim, D.L. O'Neal, Two-phase flow of Refrigerant-22 through short tube orifices, ASHRAE Trans. 100 (1) (1994) 323–334.

[9] V. Payne, D.L. O'Neal, Mass flow characteristics of R407C through short-tube orifices, ASHRAE Trans. 104 (3) (1998).

[10] Y. Kim, D.L. O'Neal, Two-phase flow of HCFC-22 and HFC-134a through short tube orifices. Ph.D. Thesis, Texas A&M University, Texas, The United State, 1993.

[11] G.M. Singh, P.S. Hrnjak, C.W. Bullard, Flow of refrigerant 134a through orifice tubes, Internat. J. HVAC&R Res. 7 (3) (2001) 245–262.

[12] J.R. Simões-Moreira, C.W. Bullard, Pressure drop and flashing mechanisms in refrigerant expansion devices, Internat. J. Refrig. 26 (7) (2003) 840–848.

[13] G. Lorentzen, Revival of carbon dioxide as a refrigerant, Internat. J. Refrig. 17 (5) (1994) 292–301.

[14] J. Süß, H. Kruse, Efficiency of the indicated process of CO_2-compressors, Internat. J. Refrig. 21 (3) (1998) 194–201.

[15] J. Pettersen, A. Hafner, G. Skaugen, H. Rekstad, Development of compact heat exchangers for CO_2 air-conditioning system, Internat. J. Refrig. 21 (3) (1998) 180–193.